Frontiers in Bioscience Landmark

Front. Biosci. (Landmark Ed) **2026**; 31(1): 45855
https://doi.org/10.31083/FBL45855

Original Research

Odaph Promotes Osteoblast Proliferation and Differentiation by Targeting the AMPK/mTOR Signaling Axis to Activate Autophagy

Yao Lin[1], Zhenzhen Xu[1], Yumin Wang[2], Haiyu Mu[3], Qing Chu[1], Wenyu Guo[1], Guolei Zhu[1], Haitao Qu[4,*], Yuguang Gao[1,*]

[1]Department of Pediatrics and Preventive Dentistry, Binzhou Medical University Hospital, 256600 Binzhou, Shandong, China
[2]Institute of Stomatology, Binzhou Medical University, 264003 Yantai, Shandong, China
[3]Department of Stomatology, Yantai Yuhuangding Hospital, Qingdao University, 264001 Yantai, Shandong, China
[4]Department of Oral and Maxillofacial Surgery, Jinan Stomatological Hospital, 250001 Jinan, Shandong, China
*Correspondence: 972165502@qq.com (Haitao Qu); gaoyuguang@bzmc.edu.cn (Yuguang Gao)
Academic Editor: Elisa Belluzzi
Submitted: 17 August 2025 Revised: 27 October 2025 Accepted: 7 November 2025 Published: 14 January 2026

Abstract

Background: Odontogenesis-associated phosphoprotein (Odaph) is essential for tooth development. However, its role in osteoblast function and bone remodeling remains unclear. Recent studies suggest that Odaph may influence bone integrity, particularly in the maxillofacial region, thereby implicating it in craniofacial skeletal disorders. The study is designed to clarify the regulatory roles of Odaph in the proliferation, differentiation, and autophagy of osteoblasts, with particular emphasis on its participation in the AMP-activated protein kinase (AMPK)/mechanistic target of rapamycin (mTOR) signaling pathway. **Methods**: The MC3T3-E1 osteoblast cell line was employed as an *in vitro* model, and the effects of Odaph overexpression on cell proliferation, differentiation, and migration were assessed via qPCR, Western blotting, CCK-8 assay, EdU staining, alkaline phosphatase (ALP) staining, and Alizarin Red S (ARS) staining. RNA sequencing (RNA-seq) was carried out to screen for differentially expressed genes, and subsequent Kyoto Encyclopedia of Genes and Genomes (KEGG)/GO enrichment analyses were conducted to verify the participation of the AMPK/mTOR signaling pathway. Autophagy was assessed via Western blotting, fluorescence double staining, transmission electron microscopy, and autophagy tandem lentiviral detection. For exploring the function of autophagy in osteogenic differentiation, the autophagy inhibitor 3-MA was used to treat the cells. Furthermore, a mouse model was utilized to confirm the impacts of Odaph overexpression on osteogenesis and autophagy *in vivo*. **Results**: Overexpression of Odaph markedly enhanced the proliferation, migration, and osteogenic differentiation of MC3T3-E1 cells, which was supported by the increased expression of osteogenic markers runt-related transcription factor 2 (RUNX2), Collagen I (COL1), and ALP. RNA-seq analysis demonstrated that genes regulated by Odaph were notably enriched in the AMPK/mTOR signaling pathway. Further validation demonstrated that Odaph increased AMPK phosphorylation while suppressing mTOR activity. Odaph overexpression also enhanced the expression of autophagy-related proteins LC3B-II and BECLIN1 while reducing p62 levels, whereas 3-MA treatment markedly attenuated these pro-osteogenic effects. Consistently, animal experiments confirmed that Odaph overexpression enhanced osteogenesis *in vivo*, accompanied by increased AMPK activation and autophagy induction. **Conclusions**: Odaph enhances osteoblast function through autophagy induction mediated by the AMPK/mTOR axis. These results reveal a new regulatory mechanism in bone biology and indicate that Odaph could serve as a potential therapeutic target for maxillofacial bone conditions, including jaw osteopenia and periodontal bone loss.

Keywords: Odontogenesis-associated phosphoprotein; osteoblasts; autophagy; MTOR signaling pathway; osteogenesis

1. Introduction

Bone formation and remodeling are tightly regulated processes governed by complex molecular signaling networks [1]. Among these, the AMP-activated protein kinase (AMPK)/mechanistic target of rapamycin (mTOR) signaling pathway exerts a central function in the maintenance of cellular energy homeostasis, metabolic adaptation, and the regulation of autophagy [2–4]. Autophagy, a degradation process mediated by lysosomes, is critical for preserving cellular homeostasis and has been increasingly acknowledged as a pivotal regulator of osteoblast differentiation and bone metabolism [5–7]. Dysregulated autophagy contributes to impaired osteogenesis and skeletal disorders such as osteoporosis [8,9]. AMPK functions as an energy sensor that suppresses mTOR following its activation, and in turn regulates osteoblast differentiation via transcription factors such as runt-related transcription factor 2 (RUNX2) and osterix (SP7) [10–14]. Moreover, AMPK activation enhances autophagic activity, which facilitates osteoblast differentiation and mineral deposition, whereas excessive mTOR activation impairs bone formation [15–18]. Although accumulating evidence connects the AMPK/mTOR pathway to osteogenesis, the upstream modulators of this axis in osteoblasts are still not well characterized.

Odontogenesis-associated phosphoprotein (Odaph) is a phosphoprotein predominantly expressed in ameloblasts

and is critical for enamel formation and hydroxyapatite mineralization [19–21]. Beyond enamel, Odaph has been associated with epithelial integrity and cell–matrix adhesion, implying potential relevance in bone-forming cells [22–24]. Given the shared mechanisms of hydroxyapatite deposition in enamel and bone, Odaph may similarly influence osteoblast differentiation. Our preliminary transcriptomic data indicated that Odaph modulates multiple genes associated with autophagy and the AMPK/mTOR signaling pathway, suggesting a potential regulatory role in skeletal metabolism. Our group has previously demonstrated that Odaph promotes osteoblast adhesion and mineralization, indicating its involvement in bone formation [19–21]. However, the molecular mechanisms through which Odaph regulates osteoblast function—particularly via autophagy and energy-sensing pathways such as AMPK/mTOR—remain unclear.

Therefore, this study sets out to explore the function of Odaph in osteoblast proliferation, differentiation, and migration, and to ascertain whether Odaph regulates osteogenesis through the AMPK/mTOR signaling axis and autophagy. By employing both MC3T3-E1 cells and osteoblast-specific Odaph-overexpressing mouse models [25], we aim to clarify the molecular mechanisms underlying Odaph-mediated regulation of bone formation, as well as its potential to serve as a therapeutic target for bone-related diseases including osteoporosis and periodontal bone loss.

2. Materials and Methods

2.1 Cell Culture

MC3T3-E1 cells (ATCC, CRL-2593) were maintained in α-MEM supplemented with 10% fetal bovine serum (FBS, A5256701, Gibco, Brazil) and 1% penicillin–streptomycin, under conditions of 37 °C in a humidified incubator with 5% CO_2. Lentiviral transduction was used to generate Odaph-overexpressing MC3T3-E1 cells, which were then selected with puromycin (2 µg/mL) for 7 days to establish stable cell lines. Prior to experimentation, all cell lines underwent validation via short tandem repeat (STR) profiling and tested negative for mycoplasma contamination.

2.2 Cell Transfection

MC3T3-E1 cells were seeded in 6-well or 12-well plates at 50–70% confluence 24 hours prior to transfection or infection. For Odaph overexpression, the Odaph overexpression lentiviral vector (Odaph-OE) and its corresponding empty vector control (Vector) were purchased from GenePharma Corporation (Shanghai, China). To achieve Odaph knockdown, Odaph-specific small interfering RNA (si-Odaph) and its matched negative control siRNA (si-NC) were obtained from GenePharma Corporation. Transfection was conducted using Lipofectamine 3000 (Invitrogen, Carlsbad, CA, USA) in accordance with the manufacturer's recommended protocol. In brief, siRNA and Lipofectamine 3000 reagent were individually diluted in Opti-MEM (Gibco, Grand Island, NY, USA) before being gently mixed. This mixture was added to the cells and incubated for 6 hours; subsequently, the transfection medium was replaced with fresh complete α-MEM supplemented with 10% fetal bovine serum.

Transduction or knockdown efficiency was assessed 48–72 hours post-treatment by qPCR and Western blotting. Expression levels of Odaph, alkaline phosphatase (ALP), Collagen I (COL1), RUNX2, and Osteocalcin (OCN) were evaluated to determine the functional effects of Odaph overexpression or silencing.

2.3 Animal Model

Eight-week-old male mice (20–23 g) from three different genotypes were used: wild-type (WT), OC-Cre $KI^{+}/^{-}$, and OC-Odaph $KI^{+}/^{+}$ mice. Mice were randomly assigned to three groups: WT, OC-Cre $KI^{+}/^{-}$, and OC-Odaph $KI^{+}/^{+}$ (n = 6 per group). WT mice, heterozygous OC-Cre knock-in (OC-Cre $KI^{+}/^{-}$) mice, and homozygous OC-Odaph knock-in (OC-Odaph $KI^{+}/^{+}$) mice were used in this study. The OC-Cre $KI^{+}/^{-}$ mice express Cre recombinase specifically in osteoblasts under the control of the osteocalcin (OC) promoter. In OC-Odaph $KI^{+}/^{+}$ mice, Odaph is overexpressed in osteoblasts as a result of Cre-mediated activation driven by the OC-Cre transgene. WT littermates lacking both knock-in alleles served as controls.

Mice were maintained under standard pathogen-free housing conditions, with free access to food and water provided ad libitum. When the mice reached 8 weeks of age, they were anesthetized to a deep state using 3% isoflurane. After deep anesthesia, CO_2 asphyxia was used for euthanasia (flow rate was 10% to 30% of the vessel volume per minute, and the concentration was 30% to 40%). Teeth were processed for Hematoxylin and Eosin (H&E) staining, immunohistochemistry (IHC) for Odaph, RUNX2, COL1, P62, LC3, p-mTOR and p-AMPK to assess the effects of the genetic modifications on dental development, osteogenesis, and autophagy. In terms of histological assessment, tissue samples were immersed in 4% paraformaldehyde for a 24-hour fixation period, subjected to decalcification in 10% EDTA for three weeks, and subsequently embedded in paraffin wax. Sections of 5 µm thickness were prepared for H&E and IHC staining. Immunohistochemical staining was performed using standard procedures and appropriate primary antibodies against Odaph, RUNX2, COL1, P62, LC3, p-mTOR and p-AMPK.

2.4 RT-qPCR

Total RNA was isolated from MC3T3-E1 cells with the TRIzol Reagent Kit (TCH021, TaKaRa Biotechnology, Kyoto, Japan), in accordance with the manufacturer's protocol. RNA concentration and purity were determined via a NanoDrop spectrophotometer. To quantify mRNA, 2 µg

of total RNA was converted to cDNA via reverse transcription using a kit from Sangong Biotech (Shanghai, China). Quantitative real-time PCR (RT-qPCR) was carried out with SYBR Green qPCR Master Mix (Vazyme, Nanjing, China). Gene expression levels were calibrated against *GAPDH* serving as the endogenous reference, and relative expression was determined with the $2^{-\Delta\Delta Ct}$ method. Primer sequences are provided in Table 1.

Table 1. qPCR primer sequence.

Name	Primer sequence: forward primers (F), reverse primers (R)
Alp	Forward: 5′-AGATGTGATGCTGAAAGAGAAAGG-3′
	Reverse: 5′-CTTTGTGAGCATACGGTCTTTG-3′
Col1	Forward: 5′-GAGCGGAGAGTACTGGATCG-3′
	Reverse: 5′-TTGAGTTTGGGTTGTTTGGA-3′
Runx2	Forward: 5′-CCGCCTCAGTGATTTAGGGC-3′
	Reverse: 5′-GGGTCTGTAATCTGACTCTGTCC-3′
Ocn	Forward: 5′-CTCACACTCCTCGCCCTATT-3′
	Reverse: 5′-GCTCCCTCATGTGTTGTCC-3′

ALP, alkaline phosphatase; COL1, Col1a1; RUNX2, runt-related transcription factor 2; OCN, Osteocalcin.

2.5 Western Blotting

Proteins were isolated from MC3T3-E1 cells with RIPA lysis buffer (Beyotime Biotechnology, Shanghai, China), which was supplemented with protease and phosphatase inhibitors (Sangong Biotech, Shanghai, China). Protein concentrations were measured using the BCA Protein Assay Kit (Beyotime Biotechnology, Shanghai, China). Equal quantities of protein samples were resolved via SDS-PAGE and then transferred to polyvinylidene fluoride (PVDF) membranes (Biosharp, Beijing, China). Membranes were blocked using 5% non-fat dry milk in TBST (Tris-buffered saline containing 0.1% Tween-20) for 1 hour at ambient temperature, followed by overnight incubation at 4 °C with primary antibodies against: anti-ALP (1:100, sc-365765, Santa Cruz, Dallas, TX, USA); anti-COL1A1 (1:1000, 72026s, Cell Signaling Technology, Danvers, MA, USA); anti-RUNX2 (1:2000, 82636-2-RR, Proteintech, Wuhan, China); anti-OCN (1:1000, 16157-1-AP, Proteintech, Wuhan, China); anti-LC3 (1:2000, 14600-1-AP, Proteintech, Wuhan, China); anti- p62(1:5000, 84826-1-RR, Proteintech, Wuhan, China); anti-Beclin 1 (1:1000, 11306-1-AP, Proteintech, Wuhan, China); anti-AMPK (1:5000, 10929-2-AP, Proteintech, Wuhan, China); anti-phospho-AMPK (P-AMPK) (1:1000, ab133448, Abcam, Cambridge, UK); anti-mTOR (1:5000, 66888-1-lg, Proteintech, Wuhan, China); anti-phospho-mTOR (P-mTOR)anti-β-actin (Proteintech, Cat No: 20536-1-AP). Following primary antibody incubation, membranes were rinsed with TBST and then incubated with HRP-conjugated secondary antibodies (Beyotime Biotechnology, Shanghai, China) for 1 hour at ambient temperature. Protein bands were detected using an enhanced chemiluminescence (ECL) detection kit (Beyotime Biotechnology, Shanghai, China). Band densities were quantified via Image J software and calibrated against β-actin.

2.6 Transwell Assays

Cell migration was evaluated using Transwell chambers (Corning Inc., Corning, NY, USA) equipped with 8µm pore size inserts. MC3T3-E1 cells (6×10^4 cells per well) were plated in the upper compartments of the Transwell, suspended in serum-free medium. The lower compartments were filled with medium containing 20% FBS, which served as a chemoattractant. Following 24 hours of incubation, non-migratory cells on the upper membrane surface were wiped off with a cotton swab, whereas migratory cells on the lower surface were fixed in 4% paraformaldehyde and stained with 0.5% crystal violet. Stained cells were imaged from at least four randomly chosen fields. The count of migrated cells was quantified using ImageJ software (National Institutes of Health, Bethesda, MD, USA). This experiment was conducted to assess how Odaph overexpression affects the migration of MC3T3-E1 cells.

2.7 Wound Healing Assay

Cell migration was further assessed via the wound healing assay. MC3T3-E1 cells (5×10^5 cells per well) were plated into 6-well plates and permitted to reach 90–95% confluence. A straight scratch was made across the monolayer of cells with a sterile 200 µL pipette tip. Following the removal of detached cells by rinsing with PBS, the cells were incubated in serum-free medium for 24 hours. Images of the wounded area were taken at 0 and 24 hours after scratching. The distance of cell migration was measured by quantifying the wound width via Image J software (National Institutes of Health, Bethesda, MD, USA). This experiment was performed to determine how Odaph overexpression influences the migratory ability of MC3T3-E1 cells.

2.8 ALP Staining Method

ALP staining was performed to assess the osteogenic differentiation of MC3T3-E1 cells. MC3T3-E1 cell suspension (2×10^4 cells per well) was seeded into a 24-well plate and incubated for 24 hours in a standard incubator. Following incubation, the culture medium was replaced with osteogenic induction medium, formulated with 50 µg/mL ascorbic acid (Beyotime, ST1434), 10 nmol/L dexamethasone (MCE, HY-14648, Shanghai, China), and 10 mmol/L β-glycerophosphate (Beyotime, ST637). After 7 days of osteogenic induction, ALP staining was performed on the cells using an ALP staining kit (Beyotime, C3206) in accordance with the manufacturer's protocol. The stained cells were examined under a bright-field microscope (OLYMPUS, BX63, Kyoto, Japan), and images were taken for subsequent analysis.

2.9 ARS Staining Method

Alizarin Red S (ARS) staining was employed to assess matrix mineralization during osteogenic differentiation. After 21 days of osteogenic induction, the cells were immersed in 70% ethanol for a 30-minute period at ambient temperature to achieve fixation. Next, the cells were stained with a 2% Alizarin Red S solution (OriCell, ALIR-10001, Suzhou, China) for 30 minutes at ambient temperature. Post-staining, the cells were rinsed with distilled water to eliminate excess dye. Mineralized nodules were visualized under a bright-field microscope (OLYMPUS, BX63, Kyoto, Japan), and representative images were taken to quantify and analyze the degree of mineralization.

2.10 Transmission Electron Microscopy (TEM) Analysis of Autophagosomes

To evaluate the formation of autophagosomes in Odaph-overexpressing MC3T3-E1 cells, transmission electron microscopy (TEM) was performed. In brief, cells were immersed in 2.5% glutaraldehyde diluted in PBS for 2 hours at 4 °C. Post-fixation, the cells were rinsed three times with PBS and subjected to post-fixation with 1% osmium tetroxide for 1 hour. The specimens were then dehydrated using a graded ethanol series (50%, 70%, 90%, and 100%) and embedded in Epon resin. Thin sections (approximately 70 nm) were cut using an ultramicrotome (Leica, EM UC7, Wetzlar, Germany), stained with uranyl acetate and lead citrate, and examined under a transmission electron microscope (JEOL, JEM-1400, Kyoto, Japan). Autophagosomes were identified as double-membraned vesicles containing cytoplasmic material, and their number and morphology were analyzed in both the control and Odaph-overexpressing groups.

2.11 RNA-seq

Total RNA was isolated with the RNeasy Mini Kit (Qiagen, Hilden, Germany). RNA integrity was verified before library preparation using the TruSeq Stranded mRNA Library Prep Kit (Illumina, California, CA, USA), in accordance with the manufacturer's instructions. Libraries were initially sequenced on a NextSeq platform (75 cycles) and further sequenced on a NovaSeq 6000 system (Illumina) at HongXu Biotechnology Co., Ltd. (Shanghai, China), after dilution to 10 μM and clustering with cBot.

Clean reads were mapped to the mouse reference genome (GRCm38) via HISAT2, and gene-level read counts were acquired using HTSeq-count. Gene expression levels were computed as FPKM. Differential expression analysis was conducted with the DESeq2 R package. Genes meeting the criteria of $|\log_2 FC| > 1$ and adjusted p-value ($q < 0.05$) were regarded as significantly differentially expressed and used for downstream analyses.

2.12 Histology and Immunohistochemical Staining

Paraffin-embedded mouse tooth tissue sections were prepared according to standard protocols. To evaluate overall tissue morphology, sections were stained with H&E. Immunohistochemical staining was performed to detect ALP, Odaph, RUNX2, P62, phosphorylated AMPK (P-AMPK), LC3 and phosphorylated mTOR (P-mTOR), following previously described procedures. In brief, primary antibodies were incubated with sections at 4 °C overnight. After washing, biotinylated secondary antibodies were applied for 1 hour at 37 °C. Signal detection was achieved using 3,3′-diaminobenzidine (DAB), and the sections were counterstained with hematoxylin and permanently mounted. In the negative control group, phosphate-buffered saline (PBS) was employed in place of the primary antibody. This staining strategy was employed to evaluate osteogenic differentiation, autophagic activity, and the activation status of the AMPK/mTOR signaling pathway in Odaph-overexpressing mice.

2.13 Immunofluorescence Assay

MC3T3-E1 cells were cultured on coverslips and treated as described. Following fixation in 4% paraformaldehyde for 15 minutes, cells were made permeable using 0.1% Triton X-100 diluted in PBS for 10 minutes. To assess autophagic activity, cells were incubated with primary antibodies against LC3 (1:200, proteintech, Cat No: 18725-1-AP) and Phalloidin overnight at 4 °C. After rinsing with PBS, the cells were incubated with a FITC-conjugated secondary antibody at 37 °C for 1 hour. Nuclei were stained with DAPI for 10 minutes, and coverslips were mounted using an antifade mounting medium. The slides were visualized using a ZEISS confocal microscope. The fluorescence intensity of LC3 puncta was quantified to assess the autophagic activity in Odaph-overexpressing MC3T3-E1 cells. This assay was used to investigate the autophagy activation induced by Odaph.

2.14 Statistical Analysis

All experiments were independently repeated at least three times ($n = 3$). Data were expressed as the mean ± SD. Statistical analysis was performed with GraphPad Prism 10.0 (San Diego, CA, USA). A t test was used to test the differences between two groups, and comparisons among multiple groups were performed with a one-way analysis of variance (ANOVA) followed by Tukey's post hoc test. A p value < 0.05 was considered to be statistically significant. All data were obtained from at least three independent experiments.

3. Results

3.1 Odaph Enhances Proliferation and Osteogenic Differentiation of MC3T3-E1 Cells

To elucidate the functional role of Odaph in osteoblast proliferation and differentiation, we established both Odaph-overexpressing (OE) and Odaph-silenced (si-Odaph) MC3T3-E1 cell models. The successful regulation of Odaph expression was verified at both the protein and mRNA levels via Western blot and quantitative PCR (Fig. 1A–C, **Supplementary Fig. 1C**). EdU staining and CCK-8 assays demonstrated that Odaph overexpression markedly increased the proportion of proliferating cells and enhanced cell viability over time compared with the control group (Fig. 1D–F). Conversely, Odaph knockdown significantly decreased EdU-positive cells, indicating reduced proliferative activity (Fig. 2C). At day 7, Western blot and qPCR analyses revealed that Odaph overexpression upregulated the early osteogenic markers ALP and COL1, accompanied by intensified ALP staining (Fig. 1G,H,K). Additional staining at day 14 further identified persistent ALP activity and enhanced mineralized nodule formation in the OE group but was not significant compared to the control (**Supplementary Fig. 1A,B**). In contrast, Odaph silencing resulted in a marked decrease in ALP activity and expression levels of ALP and COL1 (Fig. 2A,E,G). By day 21, the expression levels of the late osteogenic markers RUNX2 and OCN were significantly increased in the OE group, while being markedly decreased in Odaph-silenced cells (Figs. 1I,J,2B–F). ARS staining further revealed enhanced mineralized nodule formation following Odaph overexpression and diminished mineralization after Odaph knockdown (Figs. 1L,2B).

Collectively, these results demonstrate that Odaph positively regulates both the proliferation and osteogenic differentiation of MC3T3-E1 cells. Overexpression of Odaph promotes osteogenic marker expression and matrix mineralization, whereas its silencing impairs these processes, highlighting Odaph as a critical modulator of osteoblast function.

3.2 Odaph Promotes Migration of MC3T3-E1 Cells

The effect of Odaph on the migration ability of MC3T3-E1 osteoblasts was evaluated using both wound healing and Transwell migration assays. In the wound healing assay, Odaph overexpression markedly accelerated wound closure compared with the control group, indicating enhanced migratory activity (Fig. 3A,E). Conversely, Odaph knockdown significantly delayed wound closure, suggesting impaired migration ability in si-Odaph cells (Fig. 3B,G). Consistent results were observed in the Transwell migration assay. The number of migrated cells was substantially increased in the Odaph-overexpressing (OE) group, whereas silencing Odaph markedly reduced the number of migrating MC3T3-E1 cells compared with the respective control or siNC group (Fig. 3C,D,F–H).

Taken together, these findings demonstrate that Odaph positively regulates the migratory capacity of MC3T3-E1 osteoblasts, and loss of Odaph expression suppresses cell motility. This enhanced migration ability may facilitate the early phases of osteogenesis and bone matrix remodeling.

3.3 Odaph Activates the AMPK/mTOR Signaling Pathway

To investigate the molecular mechanisms governing Odaph-mediated osteogenesis, RNA sequencing (RNA-seq) was carried out to detect differentially expressed genes (DEGs) between the control and OE groups. The volcano plot showed 2718 genes were upregulated and 4140 were downregulated in the OE group relative to the control (Fig. 4A). Hierarchical clustering analysis further demonstrated distinct transcriptomic profiles between the two groups (Fig. 4B). Kyoto Encyclopedia of Genes and Genomes (KEGG) pathway enrichment analysis revealed significant enrichment in multiple signaling cascades associated with osteogenesis, including the mTOR, PI3K–AKT and AMPK signaling pathways (Fig. 4C). In addition, visualization of the AMPK signaling pathway within the KEGG framework suggested a potential interaction between AMPK activation and downstream mTOR modulation, implicating this axis in Odaph-mediated osteogenic regulation. To verify these transcriptomic predictions, Western blot analysis was performed to assess the phosphorylation status of key components in the AMPK/mTOR axis. Overexpression of Odaph led to a significant increase in the phosphorylation of AMPK (p-AMPK) and a notable decrease in the phosphorylation of mTOR (p-mTOR). Moreover, consistent changes were observed in p-AKT and p-PI3K, indicating concurrent modulation of upstream regulators (Fig. 4D,E).

Collectively, these results demonstrate that Odaph activates AMPK signaling and suppresses mTOR phosphorylation, thereby coordinating the AMPK–mTOR axis to promote osteogenic differentiation in MC3T3-E1 cells.

3.4 Odaph Induces Autophagy

Given the observed effects of Odaph on osteogenesis, we next examined whether autophagy contributes to the underlying mechanism. Autophagy is recognized as a key regulatory mechanism in cellular homeostasis, and we proposed that Odaph may affect this process in MC3T3-E1 osteoblasts. Western blot analysis showed that Odaph overexpression led to a significant increase in the conversion of LC3-I to LC3-II, an upregulation of Beclin1, and a decrease in P62 expression, all of which indicate enhanced autophagic activity (Fig. 5A). To further confirm this, we performed immunofluorescence staining, which showed a significant rise in LC3 puncta formation in Odaph-overexpressing cells relative to the control group, accompanied by a substantial increase in fluorescence intensity (Fig. 5B). These findings were corroborated by autophagic flux analysis using the tandem mRFP-GFP-LC3

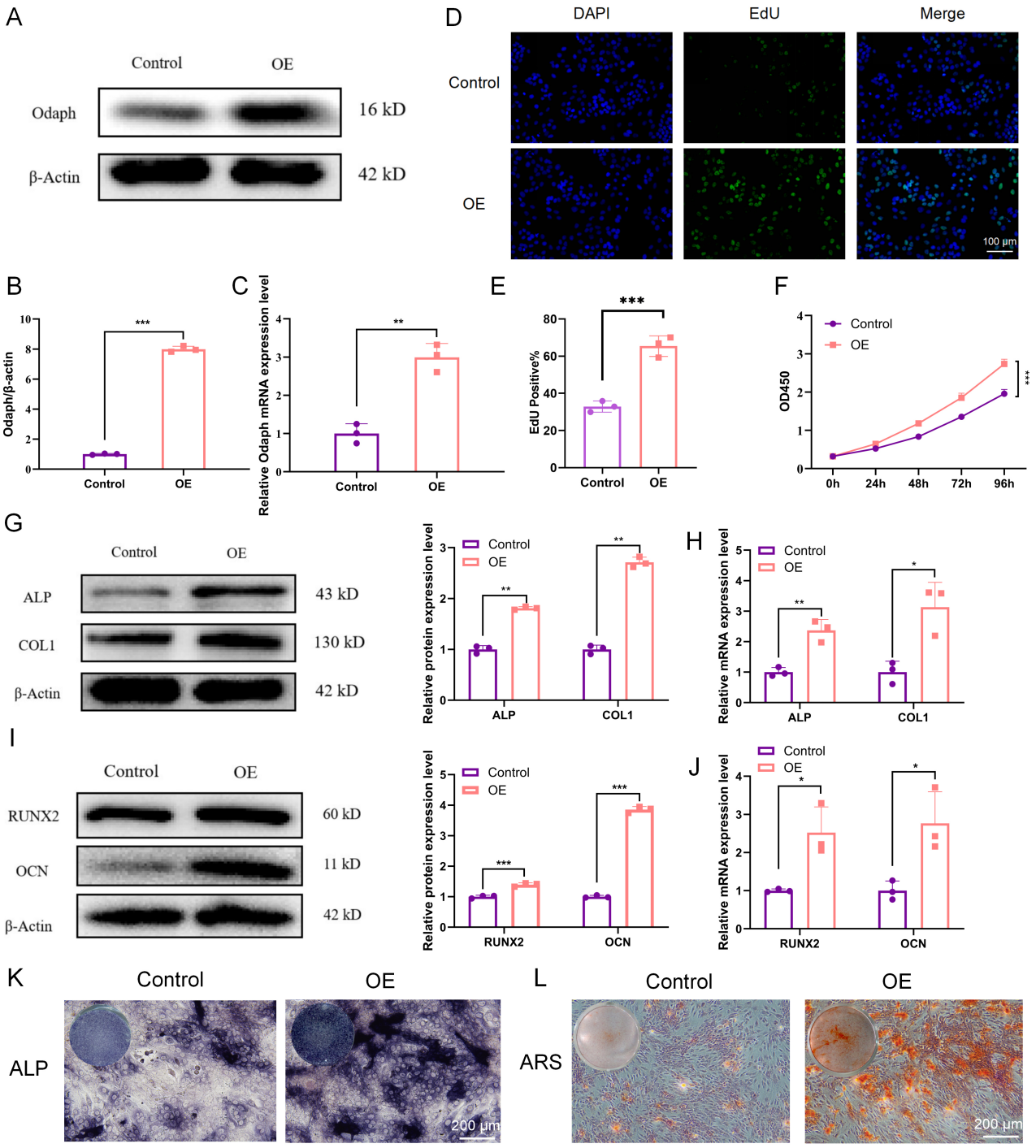

Fig. 1. Odaph overexpression promotes proliferation and osteogenic differentiation of MC3T3-E1 cells. (A,B) Western blot analysis of Odaph protein expression in MC3T3-E1 cells from the control and Odaph-overexpressing (OE) groups. (C) Quantification of Odaph protein and mRNA expression levels by qPCR, respectively. (D) Representative EdU staining images showing proliferating cells in the control and OE groups. Scale bar = 100 μm. (E) Quantification of EdU fluorescence intensity. (F) CCK-8 assay measuring cell viability at different time points. (G,H) Western blot and qPCR analyses of ALP and COL1 protein and mRNA expression levels on day 7. (I,J) Western blot and qPCR analyses of RUNX2 and OCN protein and mRNA expression levels on day 21. (K) ALP staining of MC3T3-E1 cells in the control and OE groups on day 7. Scale bar = 200 μm. (L) Alizarin Red S (ARS) staining of mineralized nodules in control and OE groups on day 21. Scale bar = 200 μm. Data are expressed as mean ± standard deviation (SD), where statistical significance is denoted as $*p < 0.05$, $**p < 0.01$, and $***p < 0.001$. ALP, alkaline phosphatase; COL1, Col1a1; RUNX2, runt-related transcription factor 2; OCN, Osteocalcin.

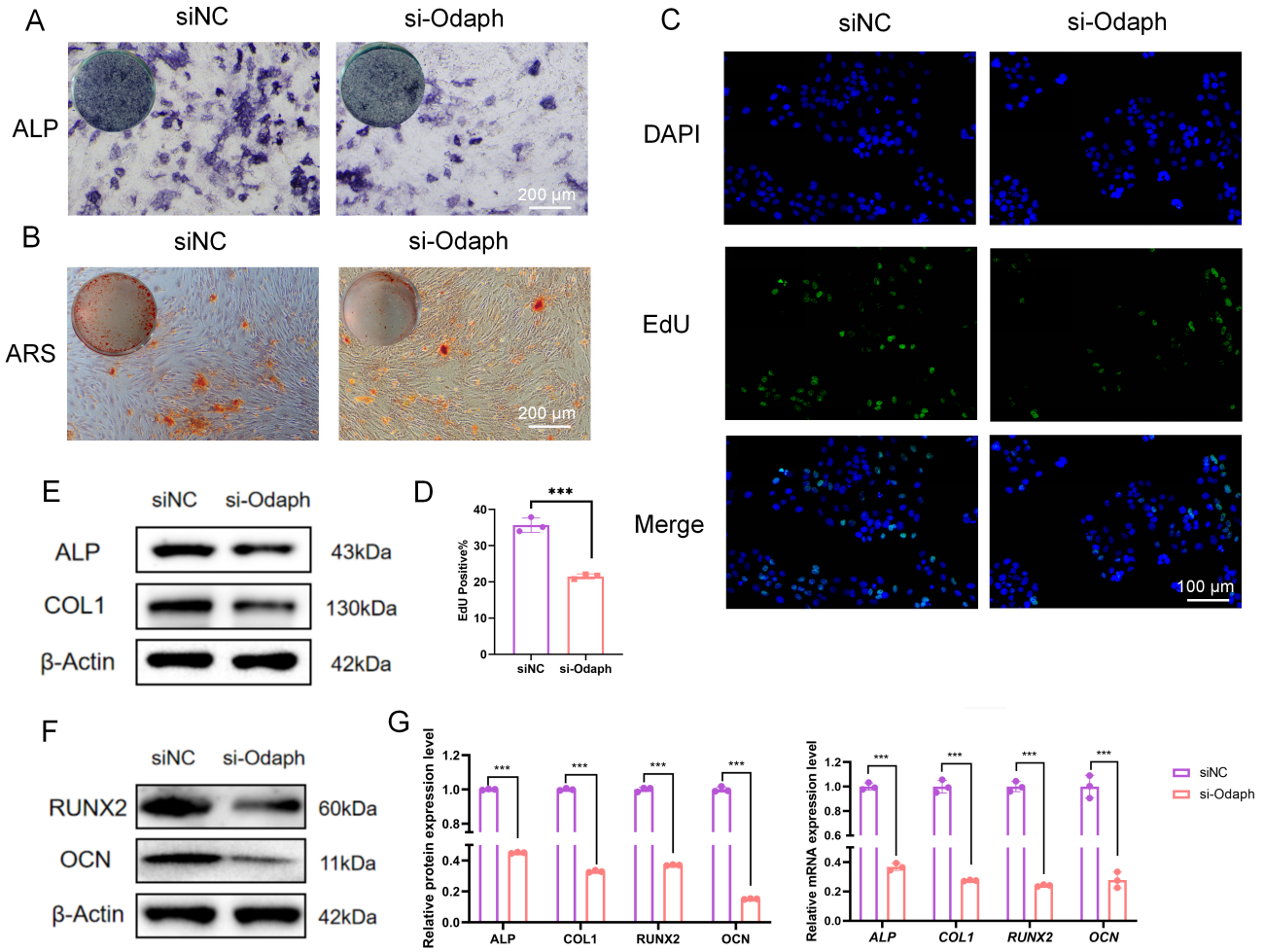

Fig. 2. Silencing of Odaph inhibits the proliferation and osteogenic differentiation of MC3T3-E1 cells. (A) ALP staining at day 7 indicating reduced alkaline phosphatase activity after Odaph knockdown. Scale bar = 200 μm. (B) ARS staining at day 21 showing diminished mineralized nodule formation in the si-Odaph group. Scale bar = 200 μm. (C,D) Representative EdU staining images showing decreased proliferative activity in Odaph-silenced cells (si-Odaph) compared with negative control (siNC). Scale bar = 100 μm. (E,F) Western blot analyses of early osteogenic markers (ALP, COL1) and late markers (RUNX2, OCN) showing significantly decreased expression levels in si-Odaph cells compared with siNC. (G) ALP, COL1 and RUNX2, OCN were quantitatively analyzed. Data are expressed as mean ± standard deviation (SD), where statistical significance is denoted as ***$p < 0.001$.

reporter system. In Odaph-overexpressing cells, we observed a significant increase in red puncta, reflecting enhanced autophagosome-lysosome fusion (Fig. 5C,D). Furthermore, transmission electron microscopy (TEM) images showed a greater accumulation of double-membrane autophagosomes in the OE group, which further supports the conclusion that Odaph enhances autophagy (Fig. 5E). Collectively, these findings indicate that Odaph has a critical role in activating autophagy in MC3T3-E1 osteoblasts.

3.5 Autophagy Inhibition Impairs the Osteogenic Differentiation-Promoting Effect of Odaph

Given the apparent role of autophagy in Odaph-mediated osteogenesis, we next examined whether autophagic activity is essential for the pro-osteogenic effects of Odaph. To address this, MC3T3-E1 cells were divided into six groups—Control, OE, 3-MA, Baf A1, OE + 3-MA, and OE + Baf A1—and treated with either 3-MA (a class III PI3K inhibitor that suppresses autophagosome formation) or Bafilomycin A1 (Baf A1) (an inhibitor of autophagosome–lysosome fusion). Western blot and qPCR analyses showed that Odaph overexpression significantly increased the expression of ALP and COL1, whereas both 3-MA and Baf A1 treatment markedly reduced these effects. The inhibitory influence was more pronounced in the combined groups (OE + 3-MA and OE + Baf A1), indicating that autophagy blockade attenuates Odaph-induced early osteogenic activation (Fig. 6A,E,G, **Supplementary Fig. 2A**). At day 21, Odaph overexpression strongly elevated RUNX2 and OCN expression, which was significantly suppressed upon treatment with either 3-MA or Baf A1 (Fig. 6B,F,H). Consistent with these molecular find-

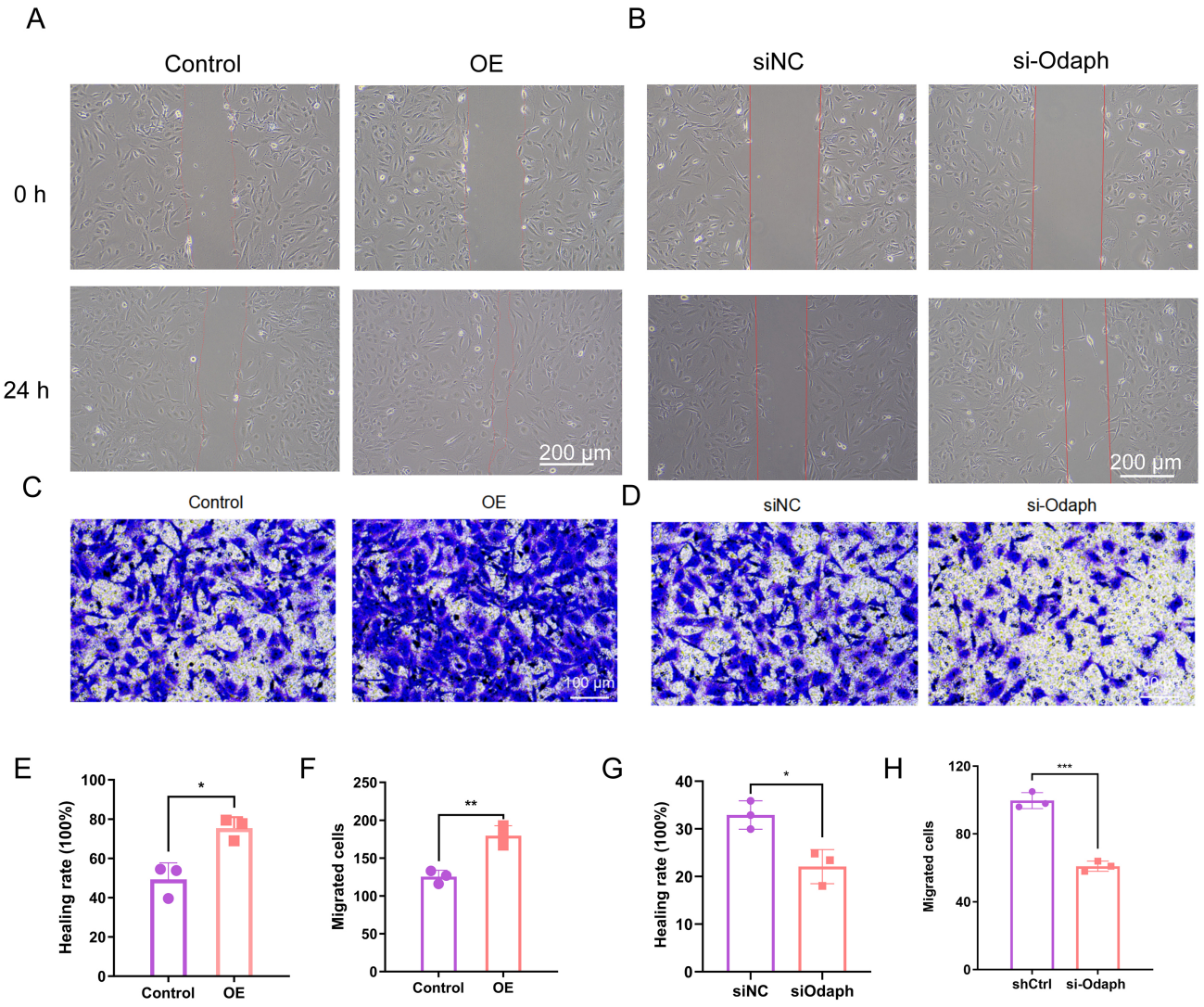

Fig. 3. Effect of Odaph on the migration ability of MC3T3-E1 osteoblasts. (A,B) Wound healing assays showing the migration of MC3T3-E1 cells in the Odaph-overexpressing (OE) and Odaph-silenced (si-Odaph) groups compared with their respective controls. The OE group exhibited accelerated wound closure, whereas the si-Odaph group showed delayed closure. Scale bar = 200 μm. (C,D) Transwell migration assays assessing the number of migrated cells in the OE and si-Odaph groups. Odaph overexpression significantly increased, while Odaph knockdown reduced, the number of migrated MC3T3-E1 cells relative to the control or siNC group. Scale bar = 100 μm. (E–H) Quantification of wound healing (E,G) and Transwell migration (F,H) assays. Statistical analyses confirmed a significant promotion of migration in Odaph-overexpressing cells and inhibition upon Odaph silencing. Data are expressed as mean ± standard deviation (SD), where statistical significance is denoted as $*p < 0.05$, $**p < 0.01$, and $***p < 0.001$.

ings, both inhibitors attenuated Odaph-induced mineralized nodule formation, as confirmed by Alizarin Red S staining (**Supplementary Fig. 2B**), supporting the essential role of autophagy in maintaining Odaph-driven osteogenic potential. Western blot analysis revealed that Odaph overexpression increased LC3-II/I ratio and Beclin1 levels while decreasing P62, indicative of enhanced autophagic flux. In contrast, treatment with 3-MA or Baf A1 reversed these effects—reducing LC3 conversion and Beclin1 expression while causing P62 accumulation (Fig. 6C,I). Consistent results were obtained from tandem GFP-LC3/mRFP-LC3 fluorescence assays, which showed that both inhibitors significantly reduced Odaph-induced autophagosome formation and flux activity (Fig. 6D,J).

Collectively, these findings demonstrate that autophagy plays a crucial role in mediating the osteogenic effects of Odaph. Pharmacological inhibition of autophagy, through either early-stage blockade (3-MA) or late-stage disruption (Baf A1), effectively abolishes the Odaph-induced enhancement of osteoblast differentiation and mineralization.

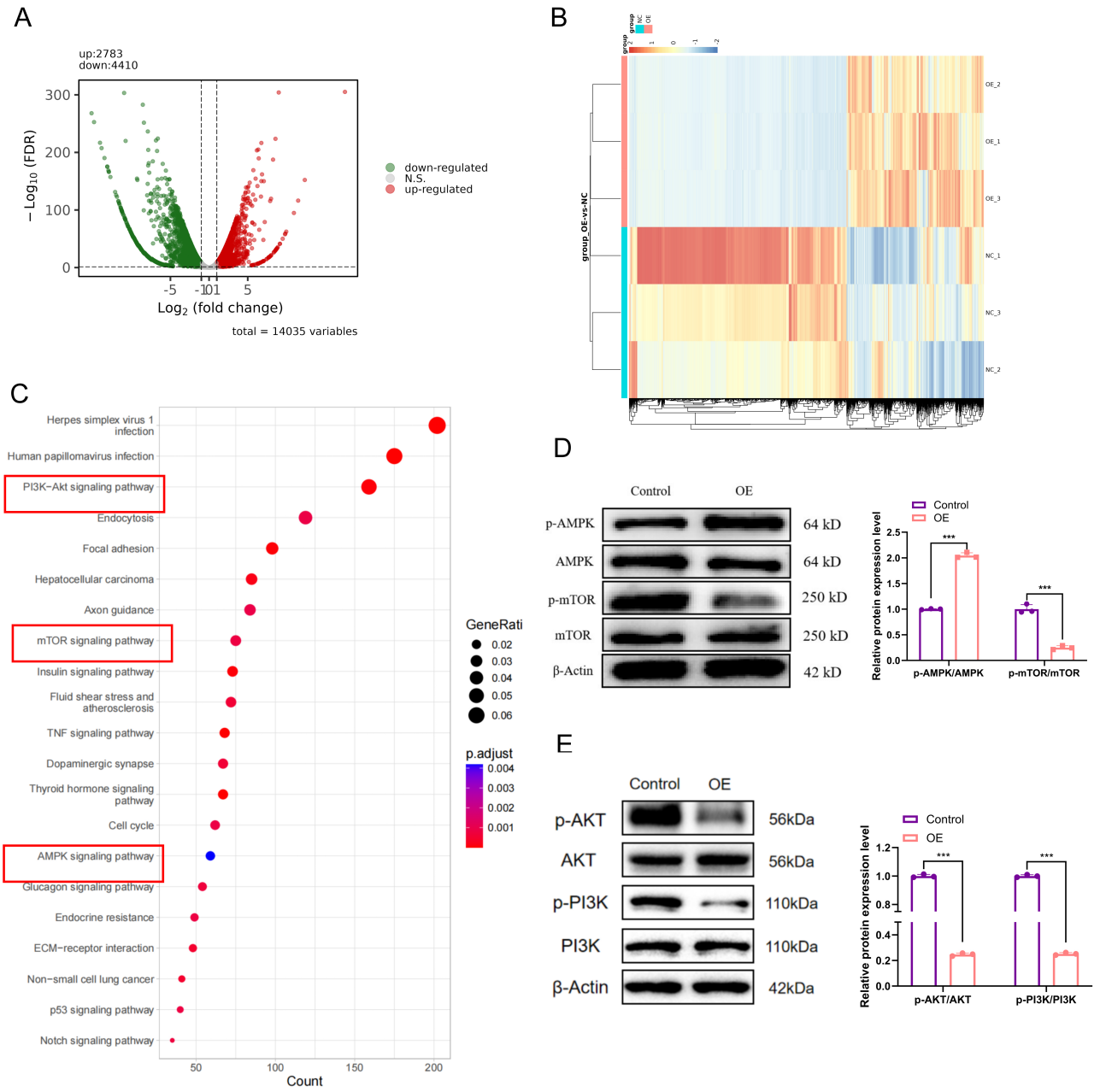

Fig. 4. Odaph activates the AMPK/mTOR signaling pathway. (A) RNA sequencing (RNA-seq) analysis detected differentially expressed genes (DEGs) between the control and Odaph-overexpression (OE) groups, which is visualized as a volcano plot. (B) Hierarchical clustering heatmap showing distinct gene expression patterns between the two groups. (C) Kyoto Encyclopedia of Genes and Genomes (KEGG) pathway enrichment analysis of DEGs, highlighting the AMPK/mTOR signaling pathway. (D) Western blot (WB) analysis of p-AMPK, p-mTOR, p-AKT and p-PI3K protein expression in control and OE groups, with (E) quantification of relative protein levels. Data are expressed as mean ± standard deviation (SD), where statistical significance is denoted as ***$p < 0.001$.

3.6 Odaph Enhances Osteogenic Differentiation and Activates Autophagy In Vivo

Lastly, to confirm the effects of Odaph on osteogenesis and autophagy *in vivo*, we developed a transgenic mouse model with osteoblast-specific Odaph overexpression and conducted histological and immunohistochemical analyses. Mice were divided into three groups: OC-Cre WT (WT), OC-Cre KI$^{+/-}$, and OC-Odaph KI$^{+/+}$. Hematoxylin-eosin (HE) staining revealed enhanced bone formation in OC-Odaph KI$^{+/+}$ mice compared to WT and OC-Cre KI$^{+/-}$ mice, indicating that Odaph overexpression promotes osteogenesis *in vivo* (Fig. 7A). Immunohistochemical staining confirmed successful Odaph overexpression (Fig. 7B and **Supplementary Fig. 3A**), with significantly increased Odaph expression in the OC-Odaph KI$^{+/+}$ group. Additionally, staining for key osteogenic markers,

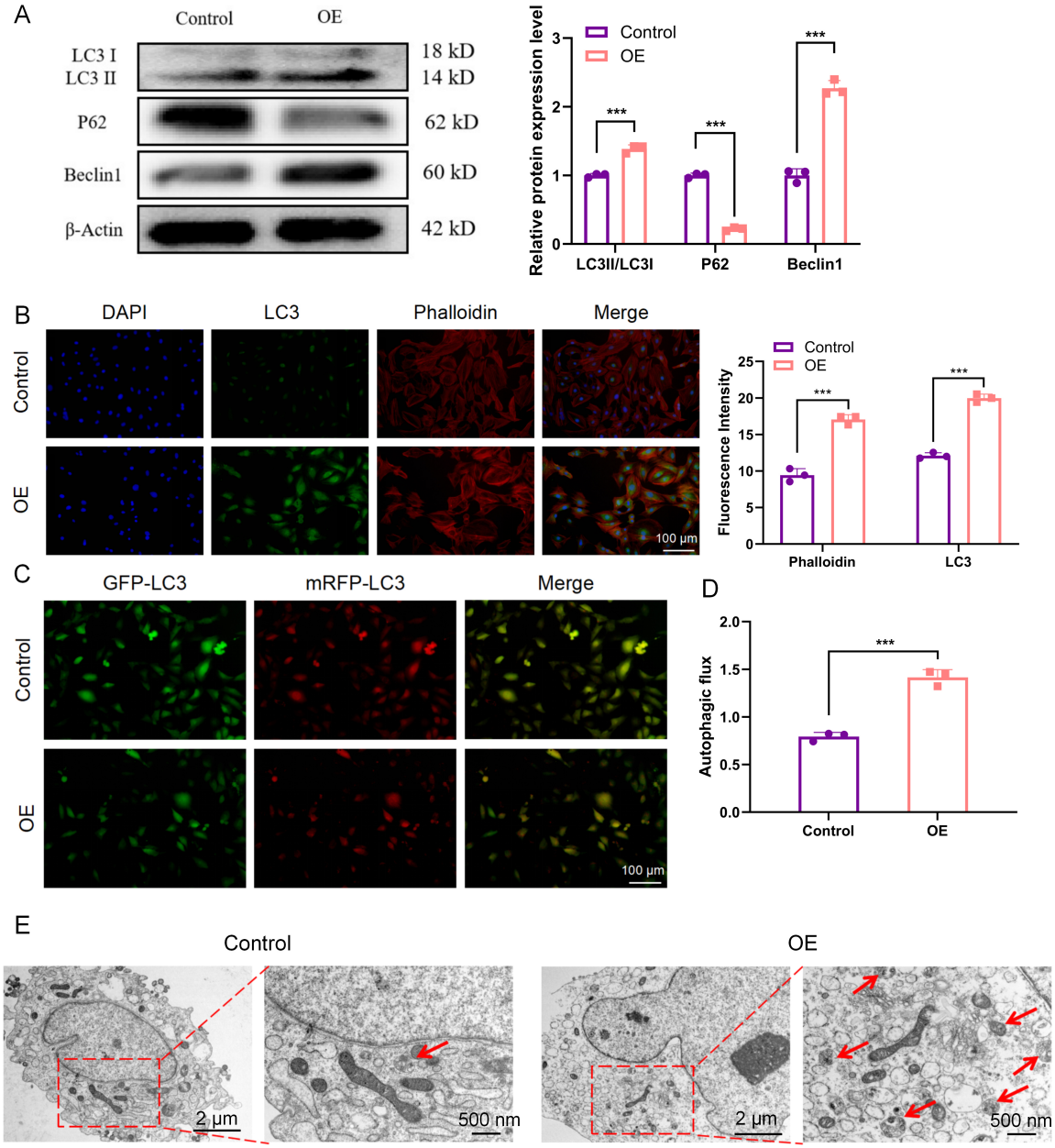

Fig. 5. Odaph overexpression induces autophagy in MC3T3-E1 cells. (A) Western blot analysis of LC3 I/II, P62, and Beclin1 protein expression in control and Odaph-overexpressing (OE) MC3T3-E1 cells, with corresponding quantification. (B) Immunofluorescence staining for LC3 (red) and phalloidin (green) in control and OE cells, with DAPI nuclear counterstaining (blue). Fluorescence intensity of phalloidin and LC3 was quantified. Scale bar = 100 μm. (C) Tandem mRFP-GFP-LC3 fluorescence imaging to assess autophagic flux, showing GFP-LC3 (green), mRFP-LC3 (red), and merged images in control and OE cells. Scale bar = 100 μm. (D) Quantification of autophagic flux based on mRFP-GFP-LC3 staining. (E) Transmission electron microscopy (TEM) images of autophagosomes (red arrows) in control and OE groups. Left: scale bar = 2 μm; right: magnified red box, scale bar = 500 nm. Data are expressed as mean ± standard deviation (SD), where statistical significance is denoted as ***$p < 0.001$.

including ALP and RUNX2, demonstrated a substantial upregulation in OC-Odaph KI$^{+/+}$ mice, further supporting that Odaph enhances osteoblast differentiation *in vivo* (Fig. 7C,D and **Supplementary Fig. 3B,C**). Considering the critical role of autophagy in osteogenesis, we evaluated LC3 and p62 expression and found that p62 levels were significantly reduced and LC3 expression was upregulated in OC-Odaph KI$^{+/+}$ mice, indicating enhanced autophagic activity (Fig. 7E,F and **Supplementary Fig. 3D,E**). To investigate the underlying signaling mechanism, we also assessed the activation of the AMPK/mTOR pathway. Immunohistochemical analysis revealed elevated phosphory-

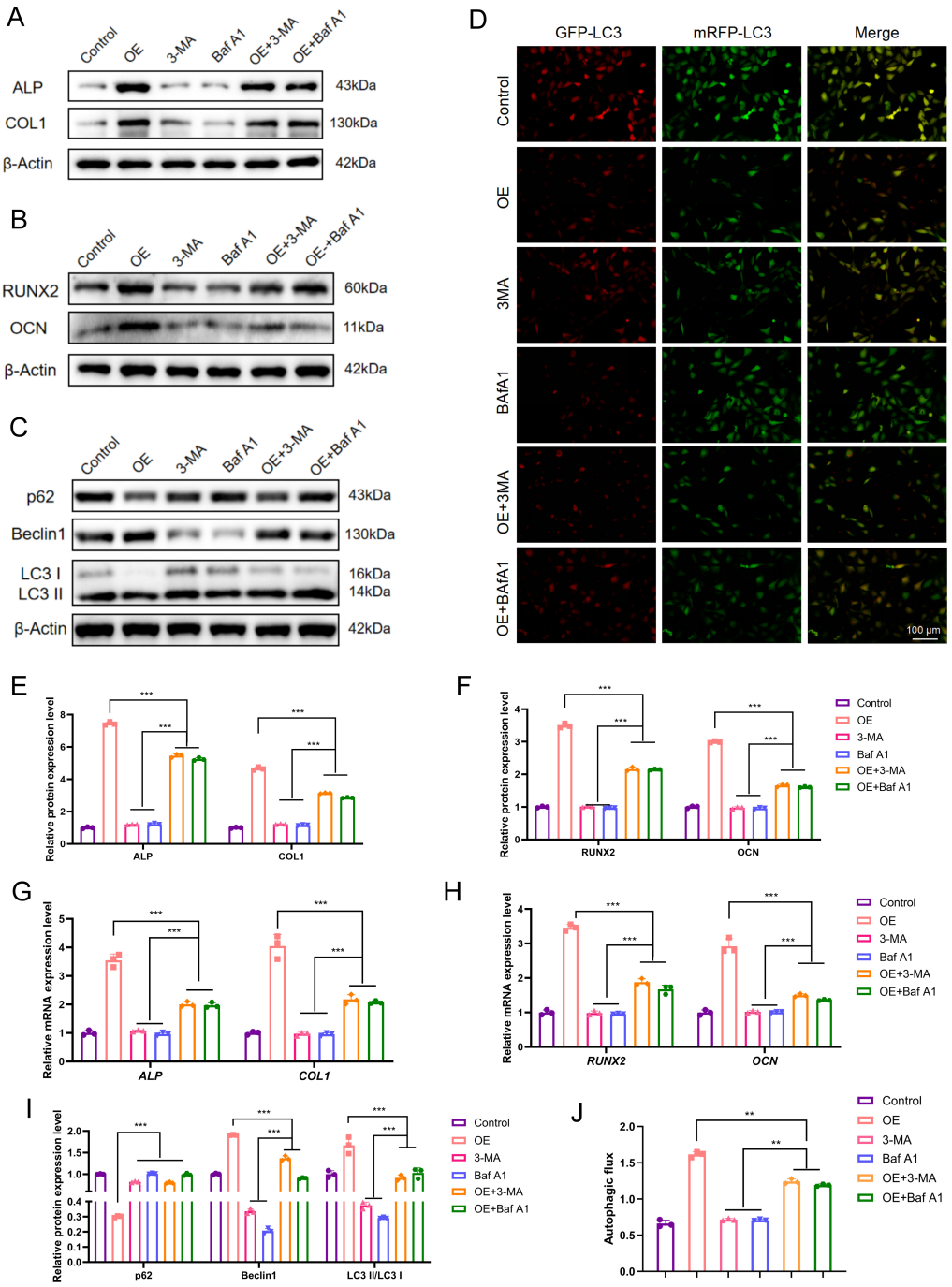

Fig. 6. Pharmacological inhibition of autophagy modulates Odaph-induced osteogenic differentiation and autophagic activity. (A) Western blot (WB) analysis of early osteogenic markers ALP and COL1 in the six indicated groups (Control, OE, 3-MA, Baf A1, OE + 3-MA, and OE + Baf A1). Both autophagy inhibitors (3-MA and Baf A1) attenuated Odaph-induced upregulation of ALP and COL1. (B) WB analysis of late-stage osteogenic markers RUNX2 and OCN at day 21 showing a similar inhibitory trend after autophagy blockade. (C) WB analysis of autophagy-related proteins LC3B, P62, and Beclin 1, with corresponding quantification of the LC3-II/I ratio, P62, and Beclin 1 levels. Odaph overexpression increased autophagic activity, whereas both inhibitors suppressed LC3 conversion and elevated P62 accumulation. (D,J) Representative fluorescence images of tandem GFP-LC3/mRFP-LC3 puncta formation in each group, with quantification of autophagic flux confirming reduced autophagy upon 3-MA or Baf A1 treatment. (E,F,I) ALP, COL1, RUNX2, OCN, LC3B, P62, and Beclin 1 were quantitatively analyzed. (G,H) ALP, COL1 and RUNX2, OCN were detected by qPCR. Scale bar = 100 μm. Data are presented as mean ± SD (n = 3). Statistical significance: $^{**}p < 0.01$, $^{***}p < 0.001$.

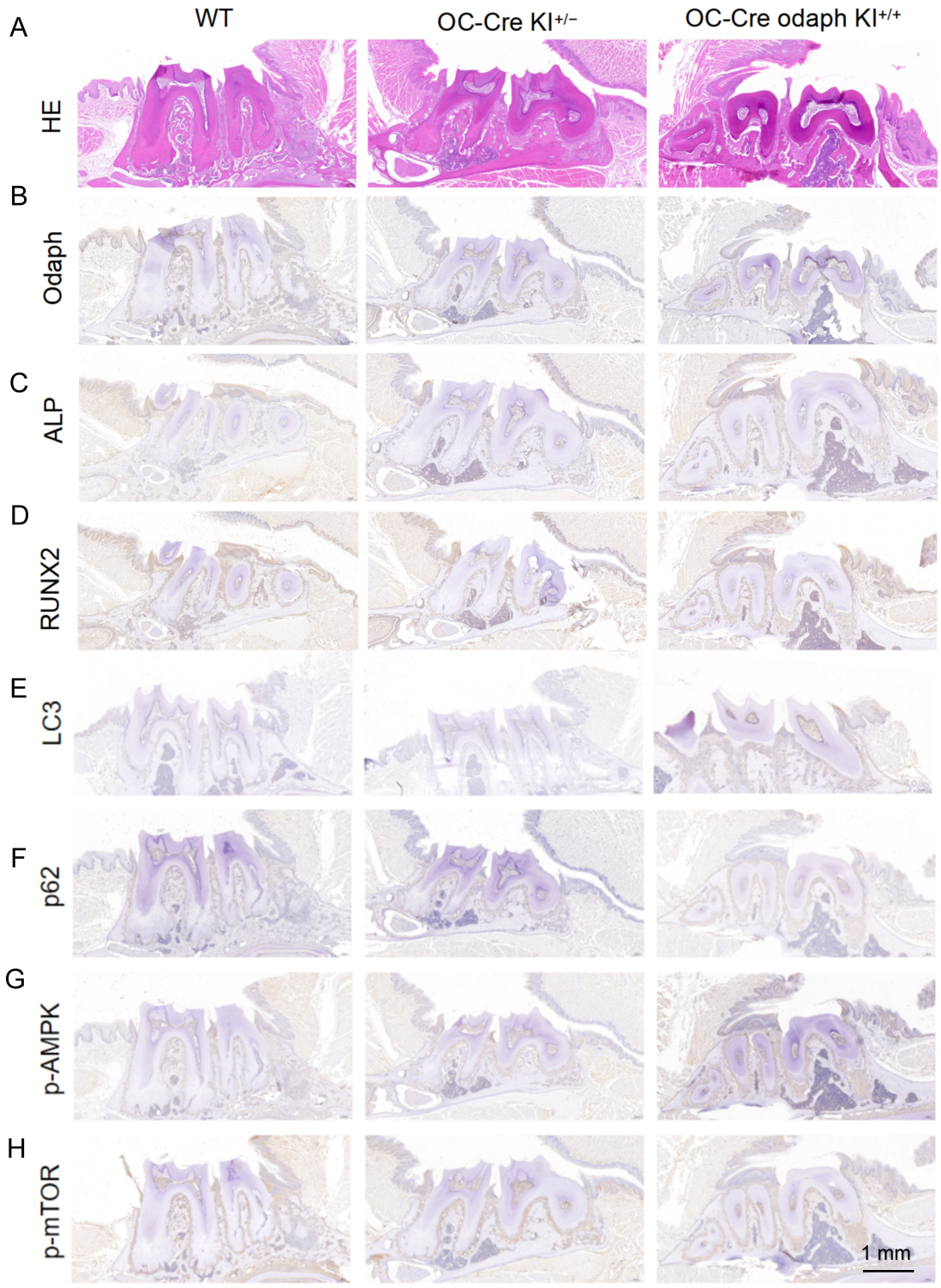

Fig. 7. Odaph enhances osteogenic differentiation and activates autophagy *in vivo*. (A) Hematoxylin-eosin (HE) staining of bone tissues from WT, OC-Cre KI$^{+/-}$ and OC-odaph KI$^{+/+}$mice. (B–H) Immunohistochemical staining of Odaph, ALP, RUNX2, p62, LC3, p-AMPK, and p-mTOR in bone tissues from WT, OC-Cre KI$^{+/-}$ and OC-odaph KI$^{+/+}$. Scale bar = 1 mm. WT, wild-type.

lation of AMPK (p-AMPK) and reduced phosphorylation of mTOR (p-mTOR) in OC-Odaph KI$^{+/+}$ mice relative to control mice, which is consistent with our *in vitro* results (Fig. 7G,H and **Supplementary Fig. 3F,G**). These results indicate that Odaph enhances osteogenesis *in vivo* by promoting autophagy through the AMPK/mTOR signaling axis. Collectively, our findings highlight that Odaph overexpression stimulates osteoblast differentiation and au-

tophagic activity *in vivo*, providing potential insights into bone formation and remodeling.

4. Discussion

In this study, we comprehensively investigated the role of Odaph in osteoblast proliferation, differentiation, migration, and autophagy, and further elucidated the molecular mechanisms underlying these effects. Our results demonstrate that Odaph enhances osteoblast proliferation, migration, and osteogenic differentiation *in vitro*, and that the effects are closely associated with activation of the AMPK–mTOR signaling axis and induction of autophagy. Importantly, transgenic overexpression of Odaph in mice confirmed its pro-osteogenic and pro-autophagic functions *in vivo*, underscoring its potential significance in bone formation and remodeling.

The enhancement of osteoblast proliferation and differentiation by Odaph observed in our *in vitro* studies is consistent with previous research that highlights the pivotal role of autophagy and metabolic signaling pathways in osteogenesis [6,8,9]. Transcriptomic profiling revealed enrichment of the mTOR and PI3K–AKT signaling pathways, while Western blot validation confirmed that Odaph activates AMPK phosphorylation and suppresses mTOR phosphorylation. The findings indicate that Odaph acts as an upstream modulator of the AMPK–mTOR axis, thereby coordinating energy metabolism and autophagic activity to facilitate osteogenic differentiation. The upregulation of LC3 and Beclin1 and decrease in P62 accumulation in Odaph-overexpressing cells further support this conclusion, consistent with enhanced autophagic flux.

Pharmacological inhibition experiments using 3-MA and Bafilomycin A1 (Baf A1) further demonstrated that autophagic activity is essential for Odaph-mediated osteogenesis [17]. Blocking autophagy at either the early (3-MA) or late (Baf A1) stages abolished Odaph-induced upregulation of ALP, COL1, RUNX2, and OCN and reduced matrix mineralization, confirming that autophagic activation is indispensable for Odaph's osteogenic effects [13]. These findings highlight a mechanistic interplay between Odaph and autophagy, suggesting that Odaph promotes osteoblast differentiation through the maintenance of active autophagic flux and metabolic balance.

Importantly, our *in vivo* data substantiate the *in vitro* findings. In transgenic mice with osteoblast-specific overexpression of Odaph, histological and immunohistochemical analyses revealed increased bone formation and elevated expression of ALP and RUNX2, confirming the pro-osteogenic function of Odaph in the physiological context. Moreover, reduced LC3 and P62 staining levels in bone tissue suggested enhanced autophagic activity in Odaph-overexpressing mice, while immunostaining for p-AMPK and p-mTOR indicated activation of the AMPK–mTOR signaling axis, consistent with our cellular data.

Together, these findings provide strong evidence that Odaph enhances osteogenesis *in vivo* by promoting autophagy through AMPK–mTOR–dependent mechanisms.

The enhanced migratory capacity of MC3T3-E1 cells following Odaph overexpression also suggests that Odaph may facilitate osteogenesis by promoting the migration of osteoblasts toward bone formation sites, a critical process in bone regeneration and remodeling. This observation agrees with previous studies linking cell motility to early bone healing stages and highlights Odaph as a potential regulator of osteoblast recruitment and spatial organization during tissue regeneration.

Taken together, our study demonstrates that Odaph promotes osteogenesis through dual mechanisms—stimulating osteoblast proliferation and migration while simultaneously activating autophagy via the AMPK–mTOR signaling axis.

The integration of *in vitro* and *in vivo* evidence supports a consistent regulatory framework in which Odaph-mediated autophagy contributes to efficient osteoblast differentiation and bone formation.

Given these findings, Odaph represents a promising molecular target for enhancing bone regeneration and for developing therapeutic strategies against bone-related disorders, including osteoporosis, fracture non-union, and metabolic bone diseases characterized by impaired osteoblast function.

Although this study delineated the key role of autophagy in Odaph-mediated osteogenesis, the precise molecular interactions between Odaph and upstream autophagy regulators such as LKB1 or CaMKKβ remain to be clarified.

Future studies employing genetic knockout or co-immunoprecipitation approaches are needed to identify potential direct interactions and delineate stage-specific regulatory mechanisms of autophagy.

Additionally, the long-term effects and safety of Odaph overexpression *in vivo* have yet to be evaluated, which will be critical for assessing its translational potential in clinical applications [14,25].

5. Conclusion

In conclusion, Odontogenesis Associated Phosphoprotein (Odaph) promotes osteoblast proliferation, migration, and differentiation both *in vitro* and *in vivo*. Mechanistically, Odaph activates the AMPK–mTOR signaling pathway and enhances autophagic flux, thereby facilitating osteogenic differentiation and bone formation. Autophagy inhibition by 3-MA or Bafilomycin A1 significantly attenuated Odaph-induced osteogenesis, confirming that autophagy is essential for its effects. Consistently, osteoblast-specific Odaph-overexpressing mice showed increased bone formation and activated AMPK–mTOR signaling, supporting the *in vivo* relevance of these findings. Collectively, Odaph functions as a positive regulator of os-

teogenesis by activating autophagy in an AMPK–mTOR-dependent manner, underscoring its potential as a therapeutic target for boosting bone regeneration and addressing metabolic bone disorders.

Availability of Data and Materials

All data supporting the results of this study are presented within the Article or **Supplementary Material**. The datasets used and analyzed during the current study are available from the corresponding author on reasonable request.

Author Contributions

YL and ZX wrote the main manuscript text. YL performed conceptualization, methodology design, formal analysis, visualization, and validation. ZX contributed to conceptualization and validation. YW supported methodology and validation. HM conducted formal analysis. WG contributed to validation. GZ and QC was responsible for investigation, resources and analyze the data. HQ and YG supervised the study and contributed to conceptualization, methodology, and manuscript revision. YG also acquired funding. All authors contributed to editorial changes in the manuscript. All authors read and approved the final manuscript. All authors have participated sufficiently in the work and agreed to be accountable for all aspects of the work.

Ethics Approval and Consent to Participate

The animal experiments involved in this study were approved by the Animal Ethics Committee of Binzhou Medical University (the animal ethics approval number: 20220128-67) in accordance with ethical principles. Experiments complied with the Guide for the Care and Use of Laboratory Animals (NIH, 8th edition), the revised Animals (Scientific Procedures) Act 1986 (UK), and Directive 2010/63/EU (EU).

Acknowledgment

Not applicable.

Funding

This study was supported by the National Natural Science Foundation of China (Grant No. 81870738) and "Clinical +X" project of Binzhou Medical University (Grant No. BY2021LCX19).

Conflict of Interest

The authors declare no conflict of interest.

Supplementary Material

Supplementary material associated with this article can be found, in the online version, at https://doi.org/10.31083/FBL45855.

References

[1] Bouzid A, Chelly A, Tekari A, Singh N, Hansdah K, Achour I, *et al*. Genetic Association of rs1021188 and DNA Methylation Signatures of *TNFSF11* in the Risk of Conductive Hearing Loss. Frontiers in Medicine. 2022; 9: 870244. https://doi.org/10.3389/fmed.2022.870244.

[2] Besterman AD, Althoff T, Elfferich P, Gutierrez-Mejia I, Sadik J, Bernstein JA, *et al*. Functional and structural analyses of novel Smith-Kingsmore Syndrome-Associated MTOR variants reveal potential new mechanisms and predictors of pathogenicity. PLoS Genetics. 2021; 17: e1009651. https://doi.org/10.1371/journal.pgen.1009651.

[3] Zinnah KMA, Seol JW, Park SY. Inhibition of autophagy flux by sertraline attenuates TRAIL resistance in lung cancer via death receptor 5 upregulation. International Journal of Molecular Medicine. 2020; 46: 795–805. https://doi.org/10.3892/ijmm.2020.4635.

[4] Guo Z, Chen X, Feng P, Yu Q. Short-term rapamycin administration elevated testosterone levels and exacerbated reproductive disorder in dehydroepiandrosterone-induced polycystic ovary syndrome mice. Journal of Ovarian Research. 2021; 14: 64. https://doi.org/10.1186/s13048-021-00813-0.

[5] Bergmann CA, Beltran S, Vega-Letter AM, Murgas P, Hernandez MF, Gomez L, *et al*. The Autophagy Protein Pacer Positively Regulates the Therapeutic Potential of Mesenchymal Stem Cells in a Mouse Model of DSS-Induced Colitis. Cells. 2022; 11: 1503. https://doi.org/10.3390/cells11091503.

[6] Liu F, Fang F, Yuan H, Yang D, Chen Y, Williams L, *et al*. Suppression of autophagy by FIP200 deletion leads to osteopenia in mice through the inhibition of osteoblast terminal differentiation. Journal of Bone and Mineral Research: the Official Journal of the American Society for Bone and Mineral Research. 2013; 28: 2414–2430. https://doi.org/10.1002/jbmr.1971.

[7] Zhang S, Zhou H, Kong N, Wang Z, Fu H, Zhang Y, *et al*. l-cysteine-modified chiral gold nanoparticles promote periodontal tissue regeneration. Bioactive Materials. 2021; 6: 3288–3299. https://doi.org/10.1016/j.bioactmat.2021.02.035.

[8] Wang J, Zhang Y, Cao J, Wang Y, Anwar N, Zhang Z, *et al*. The role of autophagy in bone metabolism and clinical significance. Autophagy. 2023; 19: 2409–2427. https://doi.org/10.1080/15548627.2023.2186112.

[9] Behera J, Ison J, Tyagi A, Mbalaviele G, Tyagi N. Mechanisms of autophagy and mitophagy in skeletal development, diseases and therapeutics. Life Sciences. 2022; 301: 120595. https://doi.org/10.1016/j.lfs.2022.120595.

[10] Steinberg GR, Hardie DG. New insights into activation and function of the AMPK. Nature Reviews. Molecular Cell Biology. 2023; 24: 255–272. https://doi.org/10.1038/s41580-022-00547-x.

[11] Sadria M, Layton AT. Interactions among mTORC, AMPK and SIRT: a computational model for cell energy balance and metabolism. Cell Communication and Signaling: CCS. 2021; 19: 57. https://doi.org/10.1186/s12964-021-00706-1.

[12] Tong X, Yu G, Fu X, Song R, Gu J, Liu Z. A Review of Signaling Transduction Mechanisms in Osteoclastogenesis Regulation by Autophagy, Inflammation, and Immunity. International Journal of Molecular Sciences. 2022; 23: 9846. https://doi.org/10.3390/ijms23179846.

[13] He X, Hua Y, Li Q, Zhu W, Pan Y, Yang Y, *et al*. FNDC5/irisin facilitates muscle-adipose-bone connectivity through ubiquitination-dependent activation of runt-related transcriptional factors RUNX1/2. The Journal of Biological Chemistry. 2022; 298: 101679. https://doi.org/10.1016/j.jbc.2022.101679.

[14] Stromsnes K, Fajardo CM, Soto-Rodriguez S, Kajander ERU, Lupu RI, Pozo-Rodriguez M, *et al*. Osteoporosis: Causes,

Mechanisms, Treatment and Prevention: Role of Dietary Compounds. Pharmaceuticals (Basel, Switzerland). 2024; 17: 1697. https://doi.org/10.3390/ph17121697.

[15] Chen M, Jing D, Ye R, Yi J, Zhao Z. PPARβ/δ accelerates bone regeneration in diabetic mellitus by enhancing AMPK/mTOR pathway-mediated autophagy. Stem Cell Research & Therapy. 2021; 12: 566. https://doi.org/10.1186/s13287-021-02628-8.

[16] Liu JY, Liu JX, Li R, Zhang ZQ, Zhang XH, Xing SJ, *et al*. AMPK, a hub for the microenvironmental regulation of bone homeostasis and diseases. Journal of Cellular Physiology. 2024; 239: e31393. https://doi.org/10.1002/jcp.31393.

[17] Zhang S, Xie Y, Yan F, Zhang Y, Yang Z, Chen Z, *et al*. Negative pressure wound therapy improves bone regeneration by promoting osteogenic differentiation via the AMPK-ULK1-autophagy axis. Autophagy. 2022; 18: 2229–2245. https://doi.org/10.1080/15548627.2021.2016231.

[18] Chen J, Long F. mTOR signaling in skeletal development and disease. Bone Research. 2018; 6: 1. https://doi.org/10.1038/s41413-017-0004-5.

[19] Mu H, Dong Z, Wang Y, Chu Q, Gao Y, Wang A, *et al*. Odontogenesis-Associated Phosphoprotein (ODAPH) Overexpression in Ameloblasts Disrupts Enamel Formation via Inducing Abnormal Mineralization of Enamel in Secretory Stage. Calcified Tissue International. 2022; 111: 611–621. https://doi.org/10.1007/s00223-022-01023-6.

[20] Li MY, Xiao S, Luan L, Zhang J, Gao Y, Zhang L. Research on the promotion of osteoblast adhesion and mineralization by odontogenesis-associated phosphoprotein. Journal of Oral Science Research. 2023; 39: 810–814. (In Chinese)

[21] Haitina T, Debiais-Thibaud M. Evolutionary genomics of odontode tissues. Odontodes (pp. 100–140). CRC Press. 2023.

[22] Li M, Zhang J, Xiao S, Liu X, Song S, Ye X, *et al*. Odontogenesis-associated phosphoprotein (ODAPH) Promotes Ameloblast adhesion and alkaline phosphatase (ALP) expression via LAMC2/ ITGB6/TGF-β1 signaling pathway. PLoS One. 2025; 20: e0328263. https://doi.org/10.1371/journal.pone.0328263.

[23] Theodoro LH, Garcia VG, Ervolino E, Holcroft J, McCulloch CA, Ganss B. Role of junctional epithelium in maintaining dento-gingival adhesion and periodontal health. Frontiers in Dental Medicine. 2023; 4: 1144537. https://doi.org/10.3389/fdmed.2023.1144537.

[24] Tian Y, Mu H, Dong Z, Wang Y, Gao Y, Gao Y, *et al*. The synergistic effects of TGF-β1 and RUNX2 on enamel mineralization through regulating ODAPH expression during the maturation stage. Journal of Molecular Histology. 2022; 53: 483–492. https://doi.org/10.1007/s10735-022-10060-2.

[25] Lian WS, Ko JY, Chen YS, Ke HC, Wu SL, Kuo CW, *et al*. Chaperonin 60 sustains osteoblast autophagy and counteracts glucocorticoid aggravation of osteoporosis by chaperoning RPTOR. Cell Death & Disease. 2018; 9: 938. https://doi.org/10.1038/s41419-018-0970-6.